International Journal of Solids and Structures 59 (2015) 79–89

Contents lists available at ScienceDirect

International Journal of Solids and Structures

journal homepage: www.elsevier.com/locate/ijsolstr

Influence of electric conductivity on intensity factors for cracks in functionally graded piezoelectric semiconductors

J. Sladek [a,*], V. Sladek [a], P.L. Bishay [b], F. Garcia-Sanchez [c]

[a] Institute of Construction and Architecture, Slovak Academy of Sciences, 84503 Bratislava, Slovakia
[b] The Hal and Inge Marcus School of Engineering, Saint Martin's University, Lacey, WA, USA
[c] Department of Civil Engineering, University of Malaga, 29031 Malaga, Spain

ARTICLE INFO

Article history:
Received 19 September 2014
Received in revised form 3 December 2014
Available online 19 January 2015

Keywords:
Meshless local Petrov–Galerkin method (MLPG)
Moving least-squares approximation
Piezoelectric solids
Semiconductor
Intensity factors
Static and impact loads
Impermeable conditions

ABSTRACT

Influence of electric conductivity on intensity factors for cracks in conducting piezoelectric materials is investigated. Mechanical and electric loads are considered for 2D crack problems. The electric displacement in conducting piezoelectric materials is influenced by the electron density and it is coupled with the electric current. The coupled governing partial differential equations (PDE) for stresses, electric displacement field and current are satisfied in a local weak-form on small fictitious subdomains. Nodal points are spread on the analyzed domain and each node is surrounded by a small circle for simplicity. Local integral equations are derived for a unit function as the test function on circular subdomains. All field quantities are approximated by the moving least-squares (MLS) scheme. Interaction integral method is developed for evaluating the intensity factors in functionally graded conducting piezoelectric materials.

1. Introduction

Functionally graded materials (FGMs) could be applied to reduce the stress concentration and increase the fracture toughness (Suresh and Mortensen, 1998; Paulino et al., 2003). Consequently, the original concept of elastic FGMs can be extended to piezoelasticity to obtain piezoelectric (PE) materials with high strength, high toughness, low thermal expansion coefficient and low dielectric constant. PE materials can be either dielectrics or semiconductors. Up to date dielectric materials are more intensively investigated than semiconductors. The solution of the boundary value problems for continuously nonhomogeneous PE solids requires advanced numerical methods due to the high mathematical complexity. The governing equations are more complicated than in a homogeneous counterpart and the electric and mechanical fields are coupled with each other. Therefore, only few crack problems in non-conducting PE medium were studied in homogeneous bodies. Pak (1990) obtained the closed-form solutions for an infinite PE medium under an anti-plane loading by using a complex variable method. Later, Park and Sun (1995) obtained closed-form solutions for all the three fracture modes associated with a crack in an infinite PE medium. They investigated the effects of the electric field on the fracture of PE ceramics. General computational methods like the finite element method (FEM) (Gruebner et al., 2003; Govorukha and Kamlah, 2004; Enderlein et al., 2005; Kuna, 2006) and the boundary element method (BEM) (Pan, 1999; Davi and Milazzo, 2001; Gross et al., 2005; Garcia-Sanchez et al., 2005, 2007; Sheng and Sze, 2006; Lei et al., 2014) need to be applied for general crack analyses in PE solids. Recently, the extended FEM has been applied for crack analyses in non-conducting PE under thermal or dynamic load (Liu et al., 2013, 2014; Bui and Zhang, 2012). In recent years, meshless formulations are becoming popular due to their high adaptivity and low costs in preparation of input and output data for numerical analyses. A variety of meshless methods has been proposed so far and some of them are also applied to PE problems (Ohs and Aluru, 2001; Liu et al., 2002; Sladek et al., 2007, 2010, 2012). Even continuously varying PE material properties are considered in some numerical analyses for non-conducting dielectric PE (Sladek et al., 2007). The results in numerical examples showed a strong dependence of the stress intensity factor (SIF) and electrical displacement intensity factor (EDIF) on material properties. Furthermore, an impact load would lead to a dynamic overshoot of the static intensity factors. A gradation of material properties affects both intensity factors.

In PE semiconductors (conducting PE) the induced electric field produces electric current. The interaction between mechanical

* Corresponding author. Tel.: +421 2 54788662; fax: +421 2 54773548.
E-mail address: jan.sladek@savba.sk (J. Sladek).

http://dx.doi.org/10.1016/j.ijsolstr.2015.01.012
0020-7683/

fields and mobile charges in piezoelectric semiconductors is called the acoustoelectric effect (Hutson and White, 1962; White, 1962). An acoustic wave traveling in a PE semiconductor can be amplified by application of an initial or biasing dc electric field (Yang and Zhou, 2005). This phenomenon is utilized in many acoustoelectric devices (Heyman, 1978; Busse and Miller, 1981). There are only few papers devoted to crack problems in piezoelectric semiconductor materials. These papers are concerned with only the anti-plane crack problem in unbounded domain with a semi-infinite crack (Yang, 2005) or a finite crack (Hu et al., 2007) under stationary conditions. The Fourier transform technique was applied to reduce the problem to a pair of dual integral equations. In the present paper, we aim at analyzing the in-plane crack problem in bounded domains under mechanical and electric loads. Static and transient boundary conditions are considered here. The meshless local Petrov–Galerkin (MLPG) method (Sladek et al., 2013) is developed for the solution of initial-boundary value problems in conducting piezoelectric solids. Nodal points are introduced and spread on the analyzed domain and each node is surrounded by a small circle for simplicity, but without loss of generality. The spatial variations of the displacement, electric potential and electron density are approximated by the moving least-squares (MLS) scheme (Zhu et al., 1998). After performing spatial integrations, a system of ordinary differential equations for the unknown nodal values is obtained. The essential boundary conditions on the global boundary are satisfied by collocation. Then, the system of ordinary differential equations of the second order resulting from the equations of motion is solved by the Houbolt finite-difference scheme (Houbolt, 1950).

2. Local integral equations for piezoelectric semiconductor

Consider a continuously nonhomogeneous n-type piezoelectric semiconductor with electron density M_0 in the unloaded state with vanishing initial electric field E_0. Generally, material properties are varying with Cartesian coordinates. One can assume quasi-static character of the first Maxwell equation, since the frequency of external loadings is significantly lower than the frequency of electromagnetic fields. The governing equations within the linear theory are given by the balance of momentum, Gauss's law and conservation of charge (Hutson and White, 1962)

$$\sigma_{ij,j}(\mathbf{x},\tau)=\rho\ddot{u}_i(\mathbf{x},\tau),\quad D_{i,i}(\mathbf{x},\tau)=qM(\mathbf{x},\tau),\quad q\dot{M}(\mathbf{x},\tau)+J_{i,i}=0, \tag{1}$$

where $\ddot{u}_i$, σ_{ij}, D_i, and q are the acceleration of elastic displacements, stress tensor, electric displacement field, and electric charge of electron, respectively. The electron density and electric current are denoted by M and J_i, respectively. Symbol ρ is used for the mass density. A comma followed by an index denotes partial differentiation with respect to the coordinate associated with the index.

The constitutive equations (Hutson and White, 1962; White, 1962) represent the coupling of the mechanical and electrical fields and electric current

$$\sigma_{ij}(\mathbf{x},\tau)=c_{ijkl}(\mathbf{x})\varepsilon_{kl}(\mathbf{x},\tau)-e_{kij}(\mathbf{x})E_k(\mathbf{x},\tau),$$

$$D_j(\mathbf{x},\tau)=e_{jkl}(\mathbf{x})\varepsilon_{kl}(\mathbf{x},\tau)+h_{jk}(\mathbf{x})E_k(\mathbf{x},\tau),$$

$$J_i(\mathbf{x},\tau)=qM_0(\mathbf{x})\mu_{ij}(\mathbf{x})E_j(\mathbf{x},\tau)-qd_{ij}(\mathbf{x})M_{,j}(\mathbf{x},\tau), \tag{2}$$

where $c_{ijkl}(\mathbf{x})$, $e_{ijk}(\mathbf{x})$, $h_{ij}(\mathbf{x})$, $\mu_{ij}(\mathbf{x})$ and $d_{ij}(\mathbf{x})$ are the elastic, piezoelectric, dielectric, electron mobility and carrier diffusion material coefficients, respectively. Generally, these coefficients can be dependent on Cartesian coordinates for the case of FGMs.

The strain tensor ε_{ij} and the electric field vector E_j are related to the displacements u_i and the electric potential ϕ by

$$\varepsilon_{ij}=\frac{1}{2}(u_{i,j}+u_{j,i}),\quad E_j=-\phi_{,j} \tag{3}$$

In the case of certain crystal symmetries, one can also formulate the plane-deformation problems (Parton and Kudryavtsev, 1988). For instance, in the crystals of hexagonal symmetry with x_3 being the 6-order symmetry axis and assuming $u_2=0$ as well as the independence on x_2, i.e. $(\bullet)_{,2}=0$, we have $\varepsilon_{22}=\varepsilon_{23}=\varepsilon_{12}=E_2=J_2=0$. Using the Voigt notation, the constitutive equations (2) are reduced to the following form

$$\begin{bmatrix}\sigma_{11}\\ \sigma_{33}\\ \sigma_{13}\end{bmatrix}=\begin{bmatrix}c_{11} & c_{13} & 0\\ c_{13} & c_{33} & 0\\ 0 & 0 & c_{44}\end{bmatrix}\begin{bmatrix}\varepsilon_{11}\\ \varepsilon_{33}\\ 2\varepsilon_{13}\end{bmatrix}-\begin{bmatrix}0 & e_{31}\\ 0 & e_{33}\\ e_{15} & 0\end{bmatrix}\begin{bmatrix}E_1\\ E_3\end{bmatrix}$$
$$\equiv\mathbf{C}(\mathbf{x})\begin{bmatrix}\varepsilon_{11}\\ \varepsilon_{33}\\ 2\varepsilon_{13}\end{bmatrix}-\mathbf{L}(\mathbf{x})\begin{bmatrix}E_1\\ E_3\end{bmatrix}, \tag{4}$$

$$\begin{bmatrix}D_1\\ D_3\end{bmatrix}=\begin{bmatrix}0 & 0 & e_{15}\\ e_3 & e_{33}0 & \end{bmatrix}\begin{bmatrix}\varepsilon_{11}\\ \varepsilon_{33}\\ 2\varepsilon_{13}\end{bmatrix}+\begin{bmatrix}h_{11} & 0\\ 0 & h_{33}\end{bmatrix}\begin{bmatrix}E_1\\ E_3\end{bmatrix}$$
$$\equiv\mathbf{G}(\mathbf{x})\begin{bmatrix}\varepsilon_{11}\\ \varepsilon_{33}\\ 2\varepsilon_{13}\end{bmatrix}+\mathbf{H}(\mathbf{x})\begin{bmatrix}E_1\\ E_3\end{bmatrix}, \tag{5}$$

$$\begin{bmatrix}J_1\\ J_3\end{bmatrix}=qM_0\begin{bmatrix}\mu_{11} & 0\\ 0 & \mu_{33}\end{bmatrix}\begin{bmatrix}E_1\\ E_3\end{bmatrix}-q\begin{bmatrix}d_{11} & 0\\ 0 & d_{33}\end{bmatrix}\begin{bmatrix}M_{,1}\\ M_{,3}\end{bmatrix}$$
$$\equiv qM_0\mathbf{A}(\mathbf{x})\begin{bmatrix}E_1\\ E_3\end{bmatrix}-q\mathbf{F}(\mathbf{x})\begin{bmatrix}M_{,1}\\ M_{,3}\end{bmatrix}. \tag{6}$$

The following essential and natural boundary conditions are assumed for the mechanical fields

$$u_i(\mathbf{x},\tau)=\tilde{u}_i(\mathbf{x},\tau),\quad \text{on}\quad \Gamma_u,$$

$$t_i(\mathbf{x},\tau)\equiv\sigma_{ij}n_j=\tilde{t}_i(\mathbf{x},\tau),\quad \text{on}\quad \Gamma_t,\Gamma=\Gamma_u\cup\Gamma_t,$$

where n_j is the unit vector normal to the boundary. For the electrical fields, we assume

$$\phi(\mathbf{x},\tau)=\tilde{\phi}(\mathbf{x},\tau),\quad \text{on}\quad \Gamma_p,$$

$$Q(\mathbf{x},\tau)\equiv D_i(\mathbf{x},\tau)n_i(\mathbf{x})=\tilde{Q}(\mathbf{x},\tau),\quad \text{on}\quad \Gamma_q,\Gamma=\Gamma_p\cup\Gamma_q,$$

and for the electric current fields

$$M(\mathbf{x},\tau)=\tilde{M}(\mathbf{x},\tau),\quad \text{on}\quad \Gamma_a,$$

$$S(\mathbf{x},\tau)\equiv J_i(\mathbf{x},\tau)n_i(\mathbf{x})=\tilde{S}(\mathbf{x},\tau),\quad \text{on}\quad \Gamma_b,\Gamma=\Gamma_a\cup\Gamma_b,$$

where Γ_u is the part of the global boundary Γ with prescribed displacements, while on Γ_t, Γ_p, Γ_q, Γ_a, and Γ_b the traction vector, electric potential, normal component of the electric displacement vector, electron density, and the electric current flux are, respectively, applied. Recall that $\tilde{Q}(\mathbf{x},\tau)$ can be considered approximately as the surface density of free charge, provided that the permittivity of the solid is much greater than that of the surrounding medium (vacuum). The summation for repeated indices is considered over 1 and 3.

The initial conditions for mechanical displacements are assumed as

$$u_i(\mathbf{x},\tau)|_{\tau=0}=u_i(x,0)\quad\text{and}\quad \dot{u}_i(\mathbf{x},\tau)|_{\tau=0}=\dot{u}_i(\mathbf{x},0)\quad\text{in}\quad\Omega.$$

The local weak form of the governing equations (1) can be written as

$$\int_{\Omega_s}[\sigma_{ij,j}(\mathbf{x},\tau)-\rho\ddot{u}_i(\mathbf{x},\tau)]u^*_{ik}(\mathbf{x})d\Omega=0, \tag{7}$$

where $u^*_{ik}(\mathbf{x})$ is a test function and $\Omega_s\subset\Omega$.

Applying the Gauss divergence theorem to the first integral and choosing the Heaviside step function as the test function $u^*_{ik}(\mathbf{x})$ in each subdomain

$$u^*_{ik}(\mathbf{x}) = \begin{cases} \delta_{ik} & \text{at} \quad \mathbf{x} \in \Omega_s \\ 0 & \text{at} \quad \mathbf{x} \notin \Omega_s \end{cases},$$

the local weak-form (7) is converted into the following local boundary-domain integral equations

$$\int_{L_s+\Gamma_{su}} t_i(\mathbf{x},\tau)d\Gamma - \int_{\Omega_s} \rho\ddot{u}_i(\mathbf{x},\tau)d\Omega = -\int_{\Gamma_{st}} \tilde{t}_i(\mathbf{x},\tau)d\Gamma, \tag{8}$$

where the boundary of the local subdomain $\partial\Omega_s$ consists of three parts $\partial\Omega_s = L_s \cup \Gamma_{st} \cup \Gamma_{su}$ (Atluri (2004)). Here, L_s is the local boundary that is totally inside the global domain, Γ_{st} is the part of the local boundary which coincides with the global traction boundary, i.e., $\Gamma_{st} = \partial\Omega_s \cap \Gamma_t$, and Γ_{su} is the part of the local boundary that coincides with the global displacement boundary, i.e., $\Gamma_{su} = \partial\Omega_s \cap \Gamma_u$. Similar definitions are valid also for other fields and related integration parts.

The local integral equation (8) is valid for both the homogeneous and nonhomogeneous solids. Nonhomogeneous material properties are included in Eq. (8) through the elastic and piezoelectric coefficients involved in the traction components

$$t_i(\mathbf{x},\tau) = [c_{ijkl}(\mathbf{x})u_{k,l}(\mathbf{x},\tau) + e_{kij}(\mathbf{x})\phi_{,k}(\mathbf{x},\tau)]n_j(\mathbf{x}).$$

Similarly, the local weak-form of the second governing equation in (1) can be written as

$$\int_{\Omega_s} [D_{j,j}(\mathbf{x},\tau) - qM(\mathbf{x},\tau)]\,v^*(\mathbf{x})d\Omega = 0, \tag{9}$$

where $v^*(\mathbf{x})$ is a test function.

Applying the Gauss divergence theorem to the local weak-form (9) and choosing the Heaviside step function as the test function $v^*(\mathbf{x})$, we obtain

$$\int_{L_s+\Gamma_{sp}} Q(\mathbf{x},\tau)d\Gamma - \int_{\Omega_s} qM(\mathbf{x},\tau)d\Omega = -\int_{\Gamma_{sq}} \tilde{Q}(\mathbf{x},\tau)d\Gamma, \tag{10}$$

where

$$Q(\mathbf{x},\tau) = D_j(\mathbf{x},\tau)n_j(\mathbf{x}) = [e_{jkl}u_{k,l}(\mathbf{x},\tau) - h_{jk}\phi_{,k}(\mathbf{x},\tau)]n_j.$$

Finally, the local integral equation corresponding to the last governing equation in (1) has the form

$$\int_{L_s+\Gamma_{sa}} S(\mathbf{x},\tau)d\Gamma + \int_{\Omega_s} q\dot{M}(\mathbf{x},\tau)d\Omega = -\int_{\Gamma_{sb}} \tilde{S}(\mathbf{x},\tau)d\Gamma, \tag{11}$$

where the electric current flux is given by

$$S(\mathbf{x},\tau) = J_j(\mathbf{x},\tau)n_j(\mathbf{x}) = [-qM_0\mu_{kj}\phi_{,k}(\mathbf{x},\tau) - qd_{jk}M_{,k}(\mathbf{x},\tau)]n_j.$$

In the MLPG method, the test and trial functions are not necessarily from the same functional spaces. For internal nodes, the test function is chosen as the Heaviside step function with its support on the local subdomain. The trial functions, on the other hand, are chosen to be the moving least-squares (MLS) approximation over a number of nodes spread within the domain of influence.

3. Moving least square approximation

In general, a meshless method uses a local interpolation to represent the trial function with the values (or the fictitious values) of the unknown variable at some randomly located nodes. The moving least-squares (MLS) approximation (Lancaster and Salkauskas, 1981; Nayroles et al., 1992) used in the present analysis may be considered as one of such schemes. According to the MLS method (Atluri, 2004), the approximation of a field variable is given as

$$\mathbf{u}^h(\mathbf{x}) = \sum_{i=1}^{s} p_i(\mathbf{x})a_i(\mathbf{x}) = \mathbf{p}^T(\mathbf{x})\mathbf{a}(\mathbf{x}), \tag{12}$$

where $\mathbf{p}^T(\mathbf{x}) = \{p_1(\mathbf{x}), p_2(\mathbf{x}), \ldots p_s(\mathbf{x})\}$ is a vector of complete basis functions of order s and $\mathbf{a}(\mathbf{x}) = \{a_1(\mathbf{x}), a_2(\mathbf{x}), \ldots a_s(\mathbf{x})\}$ is a vector of unknown parameters that depend on $\mathbf{x}$. For example, in 2-D problems

$$\mathbf{p}^T(\mathbf{x}) = \{1, x_1, x_3\} \quad \text{for } s = 3,$$

and

$$\mathbf{p}^T(\mathbf{x}) = \{1, x_1, x_3, x_1^2, x_1x_3, x_3^2\} \quad \text{for } s = 6,$$

are linear and quadratic basis functions, respectively. The basis functions are not necessarily polynomials. The MLS allows introducing $r^{-1/2}$ – singularity for secondary fields at the crack-tip vicinity for modeling fracture problems (Fleming et al. (1997)). Then, the basis functions can be considered in the following form

$$\mathbf{p}^T(\mathbf{x}) = \{1, x_1, x_3, \sqrt{r}\cos(\theta/2), \sqrt{r}\sin(\theta/2), \sqrt{r}\sin(\theta/2)\sin\theta, \sqrt{r}\cos(\theta/2)\sin\theta\} \quad \text{for } s = 7,$$

where r and θ are polar coordinates with the crack-tip as the origin. The enriched basis functions given above represent all occurring terms in asymptotic expansion of displacements at the crack tip vicinity. Then, density of node distribution in such a case can be lower than that in the case of polynomial basis functions only, while getting the same accuracy of results. Only slight differences of crack opening displacements were observed in Sladek et al. (2008) at the crack tip vicinity if singularity of fields is considered or not. Quantities at the crack tip vicinity are important for an accurate evaluation of intensity factors from asymptotic expressions. In the present paper the interaction integral method is applied for evaluation of fracture parameters, where the interaction integral is computed from quantities far from the crack tip. Accordingly, basis functions proportional to $r^{-1/2}$ – singularity (in the equation above) are not considered. Only the polynomial basis functions were used.

Following the approximation (12), the approximated functions for mechanical displacements, electric potential and electron density can be written as (Atluri, 2004)

$$\mathbf{u}^h(\mathbf{x},\tau) = \sum_{a=1}^{n} N^a(\mathbf{x})\hat{\mathbf{u}}^a(\tau),$$

$$\phi^h(\mathbf{x},\tau) = \sum_{a=1}^{n} N^a(\mathbf{x})\hat{\phi}^a(\tau),$$

$$M^h(\mathbf{x},\tau) = \sum_{a=1}^{n} N^a(\mathbf{x})\hat{M}^a(\tau), \tag{13}$$

where the nodal values, $\hat{\mathbf{u}}^a(\tau) = (\hat{u}_1^a(\tau), \hat{u}_3^a(\tau))^T$, $\hat{\phi}^a(\tau)$, and $\hat{M}^a(\tau)$, are fictitious parameters for displacements, electric potential and electron density, respectively, and $N^a(\mathbf{x})$ is the shape function associated with node a. The number of nodes n used for the approximation is determined by the weight function $w^a(\mathbf{x})$. A 4th-order spline-type weight function is applied in the present work

$$w^a(\mathbf{x}) = \begin{cases} 1 - 6\left(\frac{d^a}{r^a}\right)^2 + 8\left(\frac{d^a}{r^a}\right)^3 - 3\left(\frac{d^a}{r^a}\right)^4, & 0 \leqslant d^a \leqslant r^a \\ 0, & d^a \geqslant r^a \end{cases}, \tag{14}$$

where $d^a = \|\mathbf{x} - \mathbf{x}^a\|$ and r^a is the size of the support domain. It should be noted that a smaller size of subdomains may induce larger oscillations in the nodal shape functions (Atluri, 2004). A necessary condition for a regular MLS approximation is that at least s weight functions are non-zero (i.e. $n \geqslant s$) for each sample point $\mathbf{x} \in \Omega$. This condition determines the size of the supporting domain.

Then, the traction vector $t_i(\mathbf{x},\tau)$ at a boundary point $\mathbf{x}\in\partial\Omega_s$ is approximated in terms of the same nodal values $\hat{\mathbf{u}}^a(\tau)$ as

$$\mathbf{t}^h(\mathbf{x},\tau)=\mathfrak{N}(\mathbf{x})\mathbf{C}(\mathbf{x})\sum_{a=1}^{n}\mathbf{B}^a(\mathbf{x})\hat{\mathbf{u}}^a(\tau)+\mathfrak{N}(\mathbf{x})\mathbf{L}(\mathbf{x})\sum_{a=1}^{n}\mathbf{P}^a(\mathbf{x})\hat{\phi}^a(\tau), \tag{15}$$

where the matrices $\mathbf{C}(\mathbf{x}),\mathbf{L}(\mathbf{x})$ are defined in Eq. (4), the matrix $\mathfrak{N}(\mathbf{x})$ is related to the normal vector $\mathbf{n}(\mathbf{x})$ on $\partial\Omega_s$ by

$$\mathfrak{N}(\mathbf{x})=\begin{bmatrix} n_1 & 0 & n_3\\ 0 & n_3 & n_1\end{bmatrix},$$

and finally, the matrices $\mathbf{B}^a$ and $\mathbf{P}^a$ are represented by the gradients of the shape functions as

$$\mathbf{B}^a(\mathbf{x})=\begin{bmatrix} N^a_{,1} & 0\\ 0 & N^a_{,3}\\ N^a_{,3} & N^a_{,1}\end{bmatrix},\quad \mathbf{P}^a(\mathbf{x})=\begin{bmatrix} N^a_{,1}\\ N^a_{,3}\end{bmatrix}.$$

Similarly the normal component of the electric displacement vector $Q(\mathbf{x},\tau)$ can be approximated by

$$Q^h(\mathbf{x},\tau)=\mathbf{N}_1(\mathbf{x})\mathbf{G}(\mathbf{x})\sum_{a=1}^{n}\mathbf{B}^a(\mathbf{x})\hat{\mathbf{u}}^a(\tau)-\mathbf{N}_1(\mathbf{x})\mathbf{H}(\mathbf{x})\sum_{a=1}^{n}\mathbf{P}^a(\mathbf{x})\hat{\phi}^a(\tau), \tag{16}$$

where the matrices $\mathbf{G}(\mathbf{x})$ and $\mathbf{H}(\mathbf{x})$ are defined in Eq. (5) and

$$\mathbf{N}_1(\mathbf{x})=[\,n_1\quad n_3\,].$$

Finally, the electric current flux $S(\mathbf{x},\tau)$ is approximated by

$$S^h(\mathbf{x},\tau)=-\mathbf{N}_1(\mathbf{x})qM_0\mathbf{A}(\mathbf{x})\sum_{a=1}^{n}\mathbf{P}^a(\mathbf{x})\hat{\phi}^a(\tau)-\mathbf{N}_1(\mathbf{x})q\mathbf{F}(\mathbf{x})\sum_{a=1}^{n}\mathbf{P}^a(\mathbf{x})\hat{M}^a(\tau), \tag{17}$$

with the matrices $\mathbf{A}(\mathbf{x})$, $\mathbf{F}(\mathbf{x})$ being defined in Eq. (6).

Satisfying the essential boundary conditions and making use of the approximation formulae (13), we obtain the discretized form of these boundary conditions as

$$\sum_{a=1}^{n}N^a(\mathbf{x})\hat{\mathbf{u}}^a(\tau)=\tilde{\mathbf{u}}(\mathbf{x},\tau)\quad\text{for}\quad\mathbf{x}\in\Gamma_u,$$

$$\sum_{a=1}^{n}N^a(\mathbf{x})\hat{\phi}^a(\tau)=\tilde{\phi}(\mathbf{x},\tau)\quad\text{for}\quad\mathbf{x}\in\Gamma_p,$$

$$\sum_{a=1}^{n}N^a(\mathbf{x})\hat{M}^a(\tau)=\tilde{M}(\mathbf{x},\tau)\quad\text{for}\quad\mathbf{x}\in\Gamma_a. \tag{18}$$

Furthermore, in view of the MLS-approximations (15)–(17) for the unknown quantities in the local boundary-domain integral equations (8), (10) and (11), we obtain their discretized forms as

$$\begin{aligned}&\sum_{a=1}^{n}\left[\left(\int_{L_s+\Gamma_{st}}\mathfrak{N}(\mathbf{x})\mathbf{C}(\mathbf{x})\mathbf{B}^a(\mathbf{x})d\Gamma\right)\hat{\mathbf{u}}^a(\tau)-\left(\int_{\Omega_s}\rho(\mathbf{x})N^a d\Omega\right)\hat{\mathbf{u}}^a(\tau)\right]\\&\quad+\sum_{a=1}^{n}\left(\int_{L_s+\Gamma_{st}}\mathfrak{N}(\mathbf{x})\mathbf{L}(\mathbf{x})\mathbf{P}^a(\mathbf{x})d\Gamma\right)\hat{\phi}^a(\tau)\\&\quad=-\int_{\Gamma_{st}}\tilde{\mathbf{t}}(\mathbf{x},\tau)d\Gamma,\end{aligned} \tag{19}$$

$$\begin{aligned}&\sum_{a=1}^{n}\left(\int_{L_s+\Gamma_{sq}}\mathbf{N}_1(\mathbf{x})\mathbf{G}(\mathbf{x})\mathbf{B}^a(\mathbf{x})d\Gamma\right)\hat{\mathbf{u}}^a(\tau)\\&\quad-\sum_{a=1}^{n}\left(\int_{L_s+\Gamma_{sq}}\mathbf{N}_1(\mathbf{x})\mathbf{H}(\mathbf{x})\mathbf{P}^a(\mathbf{x})d\Gamma\right)\hat{\phi}^a(\tau)-\sum_{a=1}^{n}\left(\int_{\Omega_s}qN^a(\mathbf{x})d\Omega\right)\hat{M}^a(\tau)\\&=-\int_{\Gamma_{sq}}\tilde{Q}(\mathbf{x},\tau)d\Gamma,\end{aligned} \tag{20}$$

$$\begin{aligned}&-\sum_{a=1}^{n}\left(\int_{L_s+\Gamma_{sb}}\mathbf{N}_1(\mathbf{x})qM_0\mathbf{A}(\mathbf{x})\mathbf{P}^a(\mathbf{x})d\Gamma\right)\hat{\phi}^a(\tau)\\&\quad-\sum_{a=1}^{n}\left(\int_{L_s+\Gamma_{sb}}\mathbf{N}_1(\mathbf{x})q\mathbf{F}(\mathbf{x})\mathbf{P}^a(\mathbf{x})d\Gamma\right)\hat{M}^a(\tau)\\&\quad+\sum_{a=1}^{n}\left(\int_{\Omega_s}qN^a(\mathbf{x})d\Omega\right)\dot{\hat{M}}^a(\tau)\\&\quad=-\int_{\Gamma_{sb}}\widetilde{S}(\mathbf{x},\tau)d\Gamma,\end{aligned} \tag{21}$$

which are considered on the sub-domains adjacent to the interior nodes as well as to the boundary nodes on Γ_{st}, Γ_{sq} and Γ_{sb}.

The above given system of ordinary differential equations can be rearranged in such a way that all known quantities are on the right-hand-side of an equation. Thus, in matrix form the system becomes

$$\mathbf{A}\ddot{\mathbf{F}}(\tau)+\mathbf{B}\dot{\mathbf{F}}(\tau)+\mathbf{C}\mathbf{F}(\tau)=\mathbf{Y}(\tau), \tag{22}$$

where the vector $\mathbf{F}$ contains all the unknowns to be solved for, as listed in (19)–(21).

The Houbolt method (1950) is applied for "acceleration" as a finite-difference scheme

$$\ddot{\mathbf{F}}_{\tau+\Delta\tau}=\frac{2\mathbf{F}_{\tau+\Delta\tau}-5\mathbf{F}_{\tau}+4\mathbf{F}_{\tau-\Delta\tau}-\mathbf{F}_{\tau-2\Delta\tau}}{\Delta\tau^2}, \tag{23}$$

where $\Delta\tau$ is the time step. The backward difference method is applied for the approximation of "velocities"

$$\dot{\mathbf{F}}_{\tau+\Delta\tau}=\frac{\mathbf{F}_{\tau+\Delta\tau}-\mathbf{F}_{\tau}}{\Delta\tau}. \tag{24}$$

4. Evaluation of the intensity factors in FGMs

The enthalpy for conducting piezoelectric material has to contain terms proportional to gradients of electron density, $G_i=M_{,i}$:

$$W=\frac{1}{2}c_{ijkl}\varepsilon_{ij}\varepsilon_{kl}-e_{ikl}E_i\varepsilon_{kl}-\frac{1}{2}h_{ij}E_iE_j-\frac{1}{2}qd_{ij}G_iG_j+qM_0\mu_{ij}E_jG_i. \tag{25}$$

Based on this definition, the constitutive equations (2) can be obtained from the electric enthalpy (25) as the corresponding gradients

$$\sigma_{ij}(\mathbf{x})=\frac{\partial W}{\partial\varepsilon_{ij}}=c_{ijkl}(\mathbf{x})\varepsilon_{kl}(\mathbf{x})-e_{kij}(\mathbf{x})E_k(\mathbf{x}), \tag{26}$$

$$D_j(\mathbf{x})=-\frac{\partial W}{\partial E_j}=e_{jkl}(\mathbf{x})\varepsilon_{kl}(\mathbf{x})+h_{jk}(\mathbf{x})E_k(\mathbf{x}), \tag{27}$$

$$J_i(\mathbf{x})=\frac{\partial W}{\partial G_i}=qM_0\mu_{ij}(\mathbf{x})E_j(\mathbf{x})-qd_{ij}(\mathbf{x})G_j(\mathbf{x}), \tag{28}$$

which are also the same as those given by Yang and Zhou (2005). The gradient of the electric enthalpy density (25) is given as

$$W_{,m}(\varepsilon_{ij},E_i,G_i,x_i)=\frac{\partial W}{\partial\varepsilon_{ij}}\frac{\partial\varepsilon_{ij}}{\partial x_m}+\frac{\partial W}{\partial E_i}\frac{\partial E_i}{\partial x_m}+\frac{\partial W}{\partial G_i}\frac{\partial G_i}{\partial x_m}+\left(\frac{\partial W}{\partial x_m}\right)_{expl}, \tag{29}$$

where the last term stands for the "explicit" derivative of the enthalpy density for non-homogeneous materials, which is

$$\begin{aligned}\left(\frac{\partial W}{\partial x_m}\right)_{expl}&=\frac{1}{2}c_{ijkl,m}\varepsilon_{ij}\varepsilon_{kl}-e_{ikl,m}E_i\varepsilon_{kl}-\frac{1}{2}h_{ij,m}E_iE_j-\frac{1}{2}qd_{ij,m}G_iG_j\\&\quad+qM_0\mu_{ij,m}G_iE_j.\end{aligned} \tag{30}$$

It is assumed that the initial electron density M_0 is uniform in unloaded state. Then, utilizing Eqs. (26)–(28), the gradient of the enthalpy can be rewritten in the form

$$W_{,m} = (\sigma_{ij}u_{i,m})_{,j} - \sigma_{ij,j}u_{i,m} - D_iE_{i,m} + J_iG_{i,m} + (W_{,m})_{expl}. \quad (31)$$

Bearing in mind the second equation in (3), one can write the third term in Eq. (31) as

$$D_jE_{j,m} = D_jE_{m,j} = (D_jE_m)_{,j} - D_{j,j}E_m.$$

Similarly,

$$J_iG_{i,m} = (J_iG_m)_{,i} - J_{i,i}G_m.$$

Then, the gradient of the electric enthalpy density is given as

$$(W\delta_{jm} - \sigma_{ij}u_{i,m} + D_jE_m - J_jG_m)_{,j} = -\rho\ddot{u}_iu_{i,m} + qME_m + q\dot{M}G_m + (W_{,m})_{expl}. \quad (32)$$

An integral form of Eq. (32) may be obtained upon application of the divergence theorem. If Ω is a regular bounded region enclosed by a surface Γ whose unit outward normal vector is **n**, it follows that

$$\int_\Gamma (W\delta_{jm} - \sigma_{ij}u_{i,m} + D_jE_m - J_jG_m)n_j d\Gamma = \int_\Omega -\rho\ddot{u}_iu_{i,m}d\Omega + \int_\Omega q(ME_m + \dot{M}G_m)d\Omega + \int_\Omega (W_{,m})_{expl}d\Omega. \quad (33)$$

The integral identity (33) is valid in a region where no field irregularities prevail. In the presence of a crack, the stresses at the crack-tip are singular and the displacements are discontinuous across both crack surfaces. Therefore, a cut-out along the crack with a small region at the vicinity of a crack-tip Ω_ε has to be excluded. This region is surrounded by Γ_ε as shown in Fig. 1.

The global Cartesian coordinate system is defined in such a way that the principal axes of the material orthotropy are aligned with the global coordinates. All fields σ_{ij}, u_i, D_j, E_j and G_j are regular in the region $\Omega - \Omega_\varepsilon$. The contour $\Gamma = \Gamma_0 + \Gamma_c^+ - \Gamma_\varepsilon + \Gamma_c^-$ is a closed integration path in the counter-clockwise direction. The radius ε is considered to be very small and shrinks to zero in the limiting process. The crack surfaces Γ_c^+ and Γ_c^- are assumed to be traction-free and electrically insulating, i.e., $t_i = \sigma_{ij}n_j = 0$ and $D_n = 0$, and the crack is parallel to the x_1-axis of the local Cartesian coordinate system. Then, Eq. (33) can be written as

$$\begin{aligned}\lim_{\varepsilon\to 0}\int_{\Gamma_\varepsilon}(W\delta_{jm} - \sigma_{ij}u_{i,m} + D_jE_m - J_jG_m)n_jd\Gamma &= \int_{\Gamma_0}(W\delta_{jm} - \sigma_{ij}u_{i,m} + D_jE_m - J_jG_m)n_jd\Gamma \\ &+ \int_{\Gamma_c^+}[W^+ - W^-]\delta_{2m}d\Gamma + \lim_{\varepsilon\to 0}\int_{\Omega-\Omega_\varepsilon}\rho\ddot{u}_iu_{i,m}d\Omega \\ &- \lim_{\varepsilon\to 0}\int_{\Omega-\Omega_\varepsilon}q(ME_m + \dot{M}G_m)d\Omega - \lim_{\varepsilon\to 0}\int_{\Omega-\Omega_\varepsilon}(W_{,m})_{expl}d\Omega. \end{aligned} \quad (34)$$

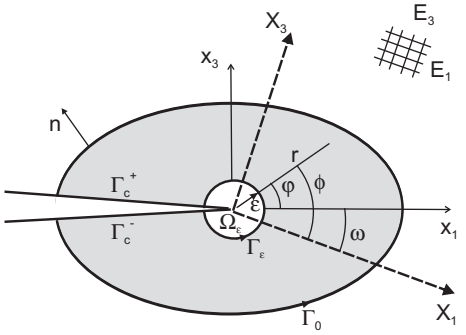

Fig. 1. Integration paths and coordinate definitions.

Hu et al. (2007) showed that the SIF and EDIF are sufficient to characterize fracture in a piezoelectric semiconductor like in a piezoelectric dielectric. However, both SIF and EDIF values are influenced by the electric current and the density of electrons in the conducting PE. Asymptotic expressions for stresses and electric intensity vector at the crack tip vicinity in both conducting and non-conducting PE are the same (Hu et al., 2007). Intensity factors (SIF and EDIF) for a crack in conducting piezoelectric materials are sufficient to characterize fracture as in the non-conducting (dielectric) ones. Then, the electromechanical *J*-integral is expressed in terms of the SIF and EDIF. Therefore, the term J_jG_m has to give a vanishing contribution on Γ_ε and the left- hand side of Eq. (34) is identical to the definition of the *J*-integral (Pak and Herrmann (1986)) for piezoelectric dielectric, denoted by A_1 [$A_1 = \lim_{\varepsilon\to 0}\int_{\Gamma_\varepsilon}(W\delta_{j1} - \sigma_{ij}u_{i,1} + D_jE_1)n_jd\Gamma$]. Then from Eq. (34), A_1 will take the following form (with $m = 1$ (Atluri, 1986)):

$$\begin{aligned}A_1 = &\int_{\Gamma_0}(W\delta_{j1} - \sigma_{ij}u_{i,1} + D_jE_1 - J_jG_1)n_jd\Gamma \\ &+ \lim_{\varepsilon\to 0}\int_{\Omega-\Omega_\varepsilon}\rho\ddot{u}_iu_{i,1}d\Omega - \lim_{\varepsilon\to 0}\int_{\Omega-\Omega_\varepsilon}q(ME_1 + \dot{M}G_1)d\Omega \\ &- \lim_{\varepsilon\to 0}\int_{\Omega-\Omega_\varepsilon}(W_{,1})_{expl}d\Omega. \end{aligned} \quad (35)$$

From the definition of the enthalpy (25) and constitutive equations (26)–(28) it is possible to show that for linear material one can write

$$W = \frac{1}{2}\sigma_{ij}\varepsilon_{ij} - \frac{1}{2}D_iE_i + \frac{1}{2}J_iG_i + \frac{1}{2}qM_0\mu_{ij}G_iE_j.$$

We now consider two independent equilibrium states in the functionally graded PE material. Let state (1) corresponds to the actual state specified by the prescribed boundary conditions (without superscript "(1)" for simplicity). Since field singularities in the conducting and non-conducting piezoelectrics are the same, the auxiliary state (2) can be selected as the asymptotic field in piezoelectric dielectrics. Superposition of the actual and auxiliary fields leads to another equilibrium state, state(s) for which the *J*-integral is given as

$$\begin{aligned}A^{(s)} = &\int_{\Gamma_0}\Big[W^{(s)}n_1 - \Big(\sigma_{ij} + \sigma_{ij}^{(2)}\Big)n_j\Big(u_{i,1} + u_{i,1}^{(2)}\Big) \\ &+ \Big(D_j + D_j^{(2)}\Big)n_j\Big(E_1 + E_1^{(2)}\Big)\Big]d\Gamma \\ &- \int_{\Gamma_0}J_jn_jG_1d\Gamma + \lim_{\varepsilon\to 0}\int_{\Omega-\Omega_\varepsilon}\rho\ddot{u}_i(u_{i,1} + u_{i,1}^{(2)})d\Omega \\ &- \lim_{\varepsilon\to 0}\int_{\Omega-\Omega_\varepsilon}q\Big[M(E_1 + E_1^{(2)}) + \dot{M}G_1\Big]d\Omega \\ &- \lim_{\varepsilon\to 0}\int_{\Omega-\Omega_\varepsilon}\Big[\frac{1}{2}c_{ijkl,1}\Big(\varepsilon_{ij} + \varepsilon_{ij}^{(2)}\Big)\Big(\varepsilon_{kl} + \varepsilon_{kl}^{(2)}\Big) \\ &- e_{ikl,1}\Big(E_i + E_i^{(2)}\Big)\Big(\varepsilon_{kl} + \varepsilon_{kl}^{(2)}\Big) - \frac{1}{2}h_{ij,1}\Big(E_i + E_i^{(2)}\Big)\Big(E_j + E_j^{(2)}\Big) \\ &- \frac{1}{2}qd_{ij,1}G_iG_j + qM_0\mu_{ij,1}G_i\Big(E_j + E_j^{(2)}\Big)\Big]d\Omega, \end{aligned} \quad (36)$$

where

$$W^{(s)} = \frac{1}{2}(\sigma_{ij} + \sigma_{ij}^{(2)})(\varepsilon_{ij} + \varepsilon_{ij}^{(2)}) - \frac{1}{2}(D_i + D_i^{(2)})(E_i + E_i^{(2)}) + \frac{1}{2}J_iG_i + \frac{1}{2}qM_0\mu_{ij}G_i\Big(E_j + E_j^{(2)}\Big).$$

Note that the auxiliary fields correspond to static case ($\ddot{u}_i^{(2)} = 0$). The *J*-integral (36) can be conveniently decomposed into

$$A^{(s)} = A_1 + A^{(2)} + T, \quad (37)$$

while A_1 will be given in Eq. (40) below, $A^{(2)}$ is defined as

$$A^{(2)} = \int_{\Gamma_0} \left[\frac{1}{2}\left(\sigma_{ij}^{(2)}\varepsilon_{ij}^{(2)} + D_i^{(2)}E_i^{(2)}\right)n_1 - \sigma_{ij}^{(2)}n_j u_{i,1}^{(2)} - D_j^{(2)}n_j E_1^{(2)}\right]d\Gamma - \lim_{\varepsilon\to 0}\int_{\Omega-\Omega_\varepsilon}\left[\frac{1}{2}C_{ijkl,1}\varepsilon_{ij}^{(2)}\varepsilon_{kl}^{(2)} - e_{ikl,1}E_i^{(2)}\varepsilon_{kl}^{(2)} - \frac{1}{2}h_{ij,1}E_i^{(2)}E_j^{(2)}\right]d\Omega, \tag{38}$$

and the interaction integral T by

$$T = \int_{\Gamma_0}\left[W^{(1,2)}n_1 - \left(\sigma_{ij}n_j u_{i,1}^{(2)} + \sigma_{ij}^{(2)}n_j u_{i,1}\right) - D_j n_j E_1^{(2)} - D_j^{(2)}n_j E_1\right]d\Gamma + lim_{\varepsilon\to 0}\int_{\Omega-\Omega_\varepsilon}\rho\ddot{u}_i u_{i,1}^{(2)}d\Omega - \lim_{\varepsilon\to 0}\int_{\Omega-\Omega_\varepsilon}qME_1^{(2)}d\Omega - \lim_{\varepsilon\to 0}\int_{\Omega-\Omega_\varepsilon}\left[\frac{1}{2}c_{ijkl,1}\left(\varepsilon_{ij}\varepsilon_{kl}^{(2)} + \varepsilon_{ij}^{(2)}\varepsilon_{kl}\right) - e_{ikl,1}\left(E_i\varepsilon_{kl}^{(2)} + E_i^{(2)}\varepsilon_{kl}\right) - \frac{1}{2}h_{ij,1}\left(E_i E_j^{(2)} + E_i^{(2)}E_j\right) + qM_0\mu_{ij,1}G_i E_i^{(2)}\right]d\Omega, \tag{39}$$

where

$$W^{(1,2)} = \frac{1}{2}\left(\sigma_{ij}\varepsilon_{ij}^{(2)} + \sigma_{ij}^{(2)}\varepsilon_{ij} - D_i E_i^{(2)} - D_i^{(2)}E_i\right) + \frac{1}{2}qM_0\mu_{ij}G_i E_j^{(2)}.$$

Intensity factors (SIF and EDIF) for a crack in conducting piezoelectric materials are sufficient to characterize fracture as in the non-conducting (dielectric) ones (Hu et al., 2007). Then, the electromechanical J-integral can be expressed in terms of the SIF and EDIF (Pak, 1990; Enderlein et al., 2005)

$$A_1 = \frac{1}{2}K_M K_N Y_{MN}, \tag{40}$$

where M and N take the summation over all the intensity factors and Y_{MN} is the Irwin matrix. If the poling direction of the material and the mechanical loading are perpendicular to the crack, only modes I and IV (D) exist. Then, the Irwin matrix Y_{MN} has a simple form and Eq. (40) is reduced to (Enderlein et al., 2005)

$$A_1 = \frac{K_I K_I}{c_T} - \frac{K_D K_D}{\kappa} + \frac{K_I K_D}{e}, \tag{41}$$

where c_T, e and κ are the effective material constants of the simplified Irwin matrix (Kuna, 2006).

For the two admissible fields (actual and auxiliary), one obtains

$$A^{(s)} = \frac{1}{c_T}\left(K_I + K_I^{(2)}\right)^2 + \frac{1}{e}\left(K_I + K_I^{(2)}\right)\left(K_D + K_D^{(2)}\right) + \frac{1}{\kappa}\left(K_D + K_D^{(2)}\right)^2 = A_1 + A^{(2)} + T,$$

where

$$A^{(2)} = \frac{1}{c_T}\left(K_I^{(2)}\right)^2 + \frac{1}{e}K_I^{(2)}K_D^{(2)} + \frac{1}{\kappa}\left(K_D^{(2)}\right)^2,$$

and

$$T = \frac{2}{c_T}K_I K_I^{(2)} + \frac{1}{e}\left(K_I K_D^{(2)} + K_I^{(2)}K_D\right) + \frac{2}{\kappa}K_D K_D^{(2)}. \tag{42}$$

Mode-I and mode-IV intensity factors are evaluated by solving the following system of linear algebraic equations

$$\frac{2}{c_T}K_I + \frac{1}{e}K_D = T^I, \tag{43}$$

$$\frac{1}{e}K_I + \frac{2}{\kappa}K_D = T^D, \tag{44}$$

resulting from Eq. (42) by taking $K_I^{(2)} = 1, K_D^{(2)} = 0$ for T^I, and $K_I^{(2)} = 0, K_D^{(2)} = 1$ for T^D, respectively. The values T^I and T^D are computed numerically by Eq. (39) with an adequate choice of the auxiliary solutions according to Park and Sun (1995), with the following fields for the PE dielectric state (state (2)):

$$u_i^{(2)}(r,\theta) = \sqrt{\frac{2r}{\pi}}\sum_{N=1}^{4}K_N d_i^N(\theta),$$

$$\phi^{(2)}(r,\theta) = \sqrt{\frac{2r}{\pi}}\sum_{N=1}^{4}K_N v^N(\theta),$$

$$\sigma_{ij}^{(2)}(r,\theta) = \frac{1}{\sqrt{2\pi r}}\sum_{N=1}^{4}K_N f_{ij}^N(\theta),$$

$$D_i^{(2)}(r,\theta) = \frac{1}{\sqrt{2\pi r}}\sum_{N=1}^{4}K_N g_i^N(\theta)$$

$$E_i^{(2)} = -\phi_{,i}^{(2)}(r,\theta). \tag{45}$$

The angular functions $f_{ij}^N(\theta)$, $g_i^N(\theta)$, $d_i^N(\theta)$ and $v^N(\theta)$ are dependent on material properties only and given by

$$f_{i1}^N = -\sum_{\alpha=1}^{4}\mathrm{Re}\left\{\frac{M_{i\alpha}N_{\alpha N}p_\alpha}{\sqrt{\cos\theta + p_\alpha\sin\theta}}\right\},$$

$$f_{i2}^N = \sum_{\alpha=1}^{4}\mathrm{Re}\left\{\frac{M_{i\alpha}N_{\alpha N}}{\sqrt{\cos\theta + p_\alpha\sin\theta}}\right\},$$

$$g_1^N = -\sum_{\alpha=1}^{4}\mathrm{Re}\left\{\frac{M_{4\alpha}N_{\alpha N}p_\alpha}{\sqrt{\cos\theta + p_\alpha\sin\theta}}\right\},$$

$$g_2^N = \sum_{\alpha=1}^{4}\mathrm{Re}\left\{\frac{M_{4\alpha}N_{\alpha N}}{\sqrt{\cos\theta + p_\alpha\sin\theta}}\right\},$$

$$d_i^N = \sum_{\alpha=1}^{4}\mathrm{Re}\left\{A_{i\alpha}N_{\alpha N}\sqrt{\cos\theta + p_\alpha\sin\theta}\right\},$$

$$v^N = \sum_{\alpha=1}^{4}\mathrm{Re}\left\{A_{4\alpha}N_{\alpha N}\sqrt{\cos\theta + p_\alpha\sin\theta}\right\},$$

where p_α are eigenvalues of the characteristic equations for an anisotropic body and the matrices $A_{i\alpha}$, $M_{i\alpha}$ and $N_{\alpha N}$ are defined in the work Park and Sun (1995).

5. Numerical examples

5.1. A central crack in a finite homogeneous strip

In the first example a straight central crack in a homogeneous finite strip under uniform mechanical and/or electrical loads is analyzed (Fig. 2). The strip is subjected to a stationary and impact loads with Heaviside time variation and the intensity $\sigma_0 = 1$ Pa for a pure mechanical load and $J_0 = 1\times10^{-10}$ Am^{-2} for a pure electric current load. The geometry of the strip is given in Fig. 2 with the following values: $a = 0.5$ m, $a/w = 0.4$ and $h/w = 1.2$ are used. Electrically impermeable boundary conditions are assumed on crack surfaces.

Due to the symmetry of the problem with respect to both Cartesian coordinates, only a quarter of the strip is modeled. We use 930 (31×30) nodes equidistantly distributed for the MLS approximation of the physical quantities. The local subdomains are considered to be circular with a radius of $r_{loc} = 0.033$ m. The material properties correspond to aluminum nitride (AlN) (Auld, 1973):

$$c_{11} = 403\times10^9\ \mathrm{Nm}^{-2},\quad c_{12} = 143\times10^9\ \mathrm{Nm}^{-2},\quad c_{13} = 104\times10^9\ \mathrm{Nm}^{-2},\quad c_{33} = 382\times10^9\ \mathrm{Nm}^{-2},$$

$$c_{44} = 120\times10^9\ \mathrm{Nm}^{-2},\quad e_{15} = -0.39\ \mathrm{Cm}^{-2},\quad e_{31} = -0.66\ \mathrm{Cm}^{-2}, e_{33} = 1.57\ \mathrm{Cm}^{-2},$$

$$h_0 = 8.854\times10^{-12}\ \mathrm{C(Vm)}^{-1},\quad h_{11} = h_{33} = 9.14\,h_0,\quad \mu_{11} = \mu_{33} = 3.0\times10^{-2}\ \mathrm{m}^2\mathrm{(Vs)}^{-1},$$

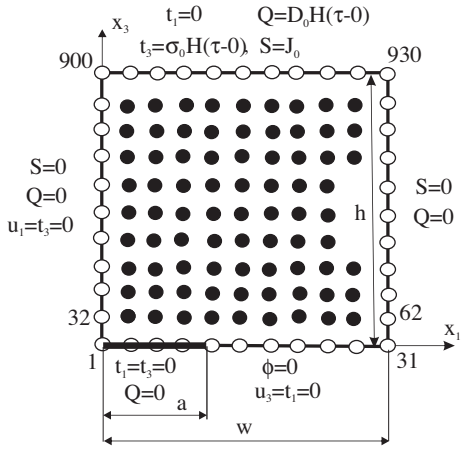

Fig. 2. Central crack in a finite homogeneous strip.

$d_{11} = d_{33} = 7.0 \times 10^{-4}$ m^2 s^{-1}, $q = 1.602 \times 10^{-19}$ C, $\rho = 3255$ kg/m^3.

Stationary boundary conditions are considered in the first example and absence of surface free electric charge $\tilde{Q} = 0$ and electric current flux $\tilde{S} = 0$ are assumed on the outer boundary. Variations of displacements, electric potentials and electron densities along the crack surface ($x_3 = 0$) for various initial electron densities M_0 are presented in Figs. 3–5, respectively. The presented numerical results correspond to a pure mechanical load (i.e., $t_3 = \sigma_0$, $D_0 = J_0 = 0$ in Fig. 2). Numerical results for non-conducting PE can be found in Sladek et al. (2007), where one can also find comparison between MLPG results and FEM results. One can observe that while the initial electron density has only a small influence on the crack displacement, it strongly affects the induced electric potential. The largest value of the induced potential is for a non-conducting PE material, and with increasing value of M_0, the induced electric potential decreases. Furthermore, the distribution of the electron density on the crack surface is also strongly dependent on M_0. The larger the value of M_0, the larger the induced density of electrons M.

The same cracked sample under pure electric current load $J_0 = 1 \times 10^{-10}$ A/m^2 and stationary conditions is investigated too. Variations of the induced displacement, electric potential and electron density on the crack surface are presented in Figs. 6–8, respectively. It is observed clearly that a larger M_0 would induce a smaller

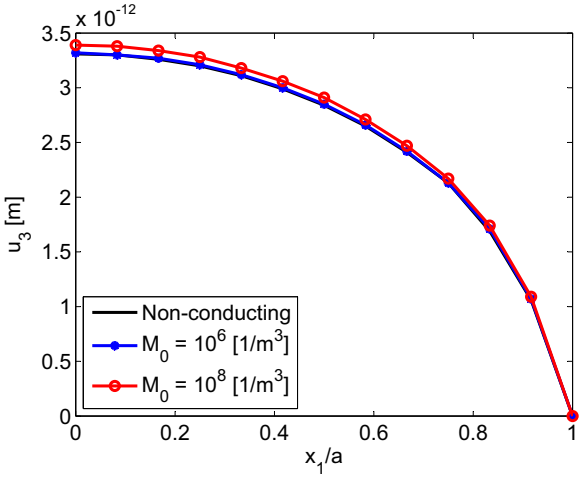

Fig. 3. Variation of the crack-opening-displacement on the crack surface with normalized coordinate x_1/a under pure mechanical load $\sigma_0 = 1$ Pa.

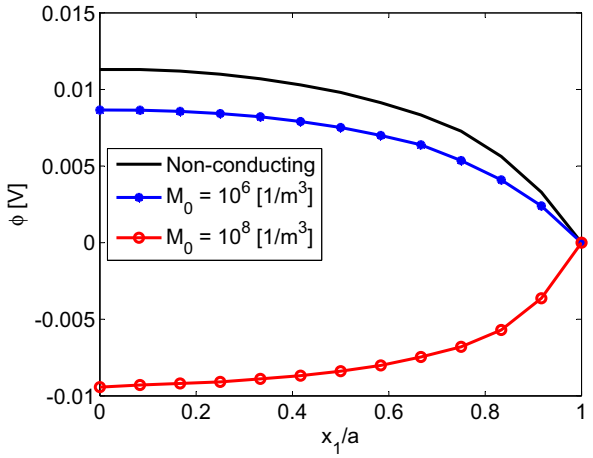

Fig. 4. Variation of the electric potential on the crack surface with normalized coordinate x_1/a under pure mechanical load $\sigma_0 = 1$ Pa.

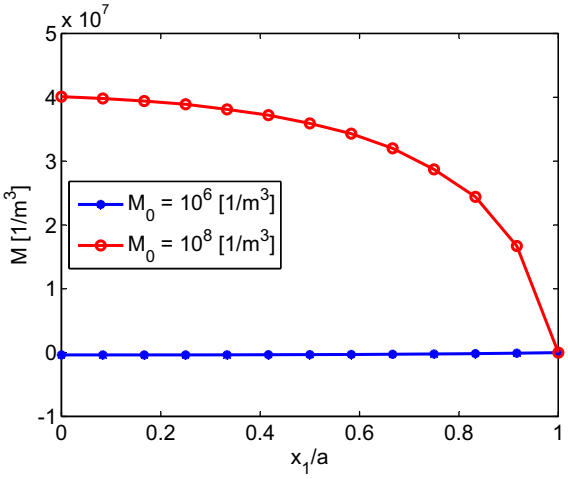

Fig. 5. Variation of the electron density M on the crack surface normalized coordinate x_1/a under pure mechanical load $\sigma_0 = 1$ Pa.

crack displacement and density of electrons M, but a larger electric potential.

For the same central crack under pure mechanical load and stationary boundary conditions in the non-conducting PE, the stress intensity factor of pure mode I is $K_I^{stat} = 1.4$ Pa m$^{1/2}$. We also obtained the same value of SIF for the cracked sample in the conducting PE. Next the influence of the non-stationary boundary conditions on the physical quantities is investigated. The same strip (Fig. 2) is subjected to an impact mechanical load with Heaviside time variation. The time variation of the normalized stress intensity factors for a non-conducting and semiconductor PE solid are presented in Fig. 9. One can observe that the initial electron density has no influence on the SIF. The normalized electrical displacement factor $\Lambda K_D/K_I^{stat}$ is presented in Fig. 10, where $\Lambda = e_{33}/h_{33}$. While the electrical displacement intensity factor for a pure static mechanical load is zero, the EDIF is not in the dynamic case with a finite velocity of wave propagation for a pure mechanical load. Furthermore, one can observe that initial electron density M_0 has a strong influence on the EDIF. A larger M_0 corresponds to a larger EDIF.

SIF and EDIF for a pure electrical displacement load are presented in Figs. 11 and 12, respectively. Contrary to the static pure mechanical load case, the SIF under static pure electrical displace-

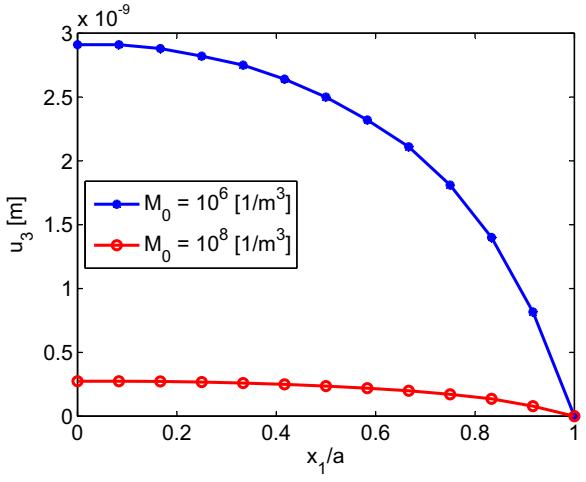

Fig. 6. Variations of the crack-opening-displacement on the crack surface with normalized coordinate x_1/a under pure electric current load $J_0 = 1 \times 10^{-10}$ A/m^2.

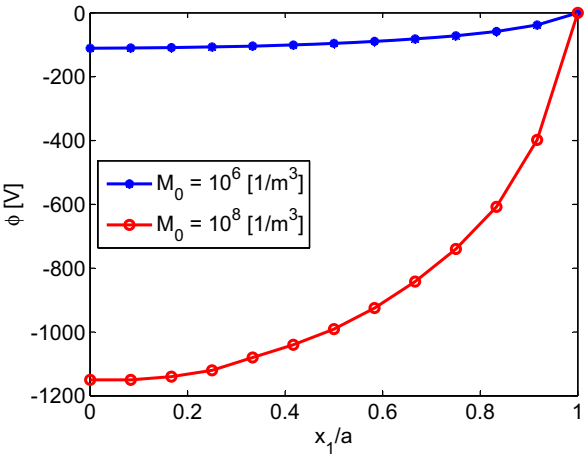

Fig. 7. Variations of the electric potential on the crack surface with normalized coordinate x_1/a under pure electric current load $J_0 = 1 \times 10^{-10}$ A/m^2.

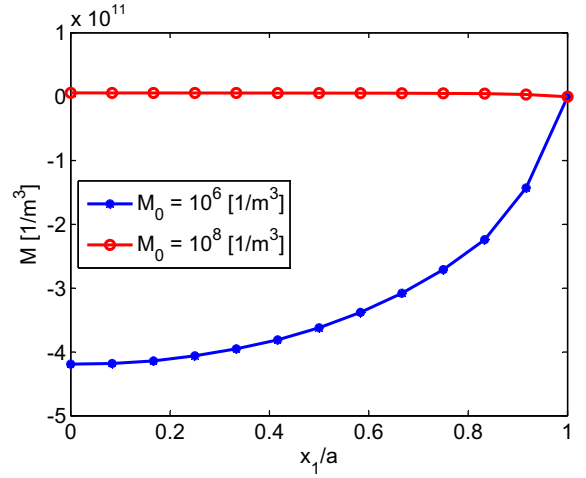

Fig. 8. Variation of the electron density M on the crack surface with normalized coordinate x_1/a under pure electric current load $J_0 = 1 \times 10^{-10}$ A/m^2.

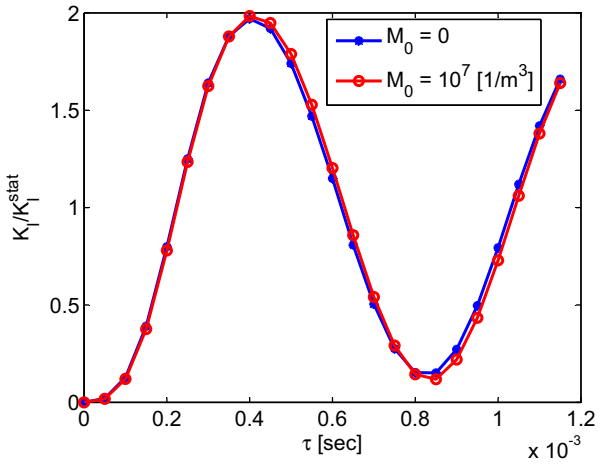

Fig. 9. Normalized stress intensity factor for a central crack in a strip under pure mechanical load.

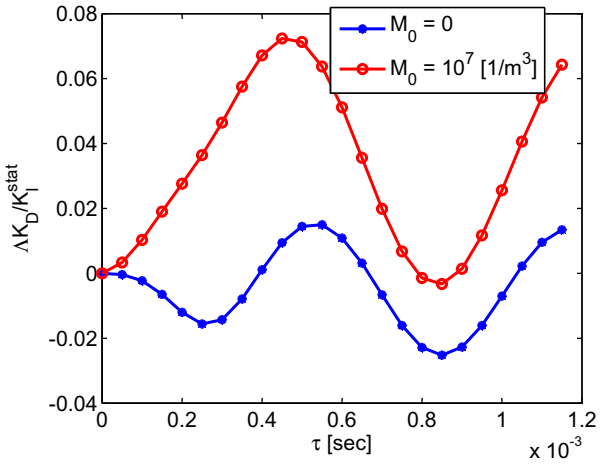

Fig. 10. Normalized electrical displacement intensity factor for a central crack in a strip under pure mechanical load.

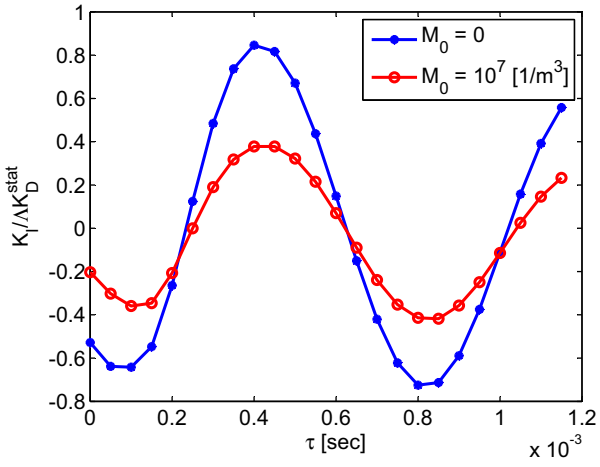

Fig. 11. Normalized stress intensity factor for a central crack in a strip under pure electrical displacement load D_0.

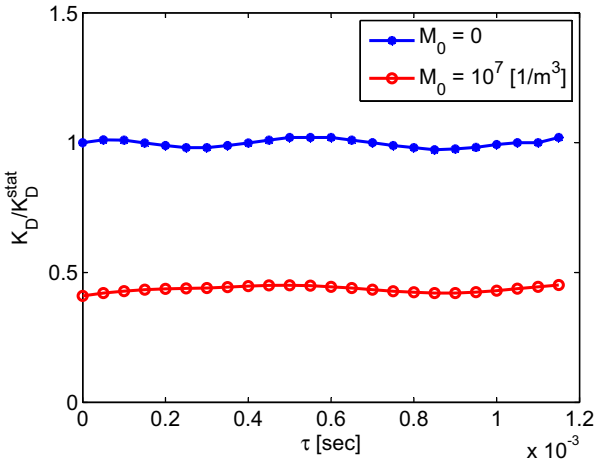

Fig. 12. Normalized electrical displacement intensity factor for a central crack in a strip under pure electrical displacement load D_0.

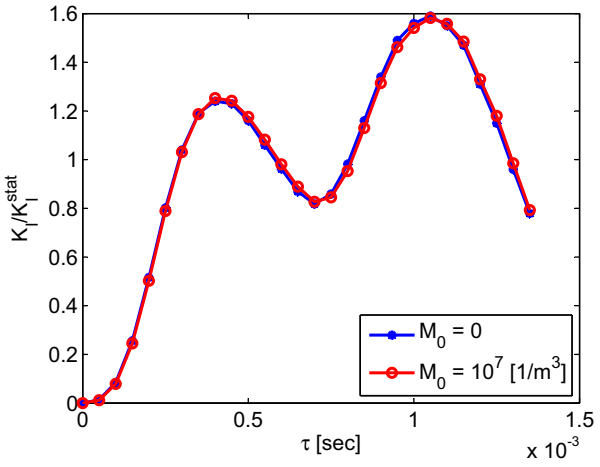

Fig. 13. Normalized stress intensity factor for edge crack in a strip under pure mechanical load.

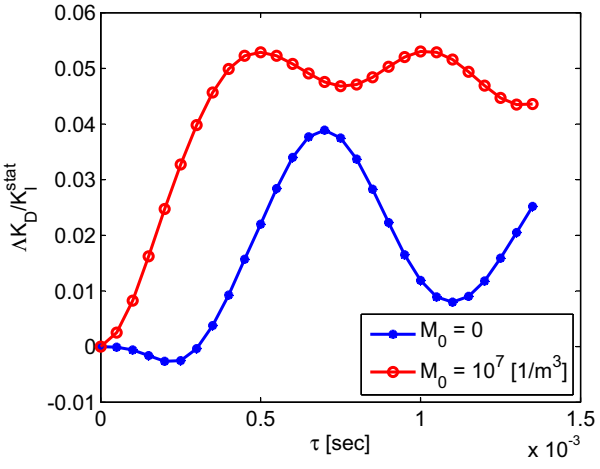

Fig. 14. Normalized electrical displacement intensity factor for edge crack in a strip under pure mechanical load.

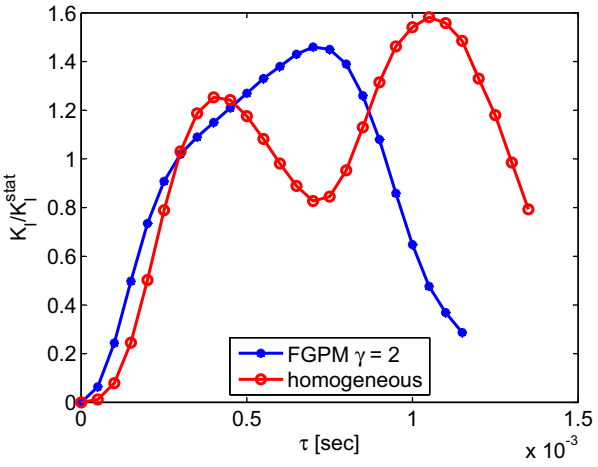

Fig. 15. Normalized stress intensity factor for edge crack in PE conducting strip with $M_0 = 1 \times 10^7$ m^{-3} under pure mechanical load.

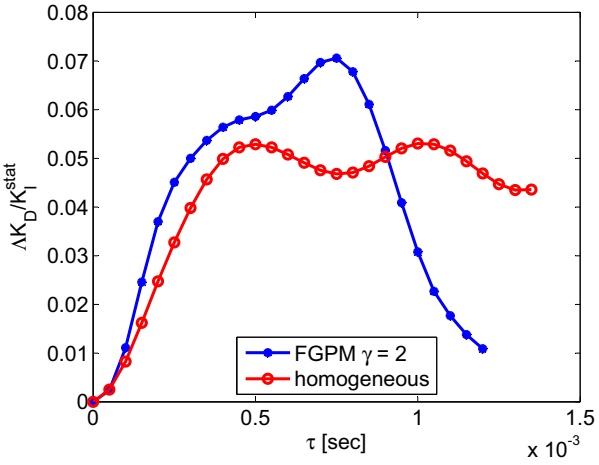

Fig. 16. Normalized electrical displacement intensity factor for edge crack in PE conducting strip with $M_0 = 1 \times 10^7$ m^{-3} under pure mechanical load.

ment load is not vanishing. This could be explained as below. From Maxwell's equations, it is known that the velocity of electromagnetic waves is equal to the speed of light, which is much greater than the velocity of elastic waves. Therefore, both SIF and EDIF are reduced in conducting PE compared to dielectric PE .

5.2. An edge crack in a finite strip

An edge crack in a finite strip is analyzed in the second example. The geometry is only the right half of the central crack case in Fig. 2 with the following geometric parameters: $a = 0.5$ m, $a/w = 0.4$ and $h/w = 1.2$. Due to the symmetry with respect to x_1-axis, only half of the specimen is modeled. The geometry is the same as in Fig. 2 but with free lateral boundary conditions on the left-hand side. Material properties are also the same as in the previous example. We have used 930 nodes equidistantly distributed for the MLS approximation of physical fields. The static stress intensity factor for the considered load and geometry is equal to $K_I^{stat} = 2.642$ Pa m$^{1/2}$. The normalized SIF and EDIF for the homogeneous cracked strip under an impact pure mechanical load are presented in Figs. 13 and 14, respectively. One can again observe that the initial electron density has a vanishing influence on SIF. However, the EDIF is strongly

dependent on the initial electron density. In the conducting PE, the EDIF is enlarged with respect to that in non-conducting PE under pure mechanical load.

5.3. An edge crack in a finite strip of functionally graded piezoelectric material

Finally, an exponential variation, characterized by the parameter γ, for the elastic, piezoelectric and dielectric tensors is considered

$$\begin{aligned} c_{ijkl}(\mathbf{x}) &= c_{ijkl0}\exp(\gamma x_1), \\ e_{ijk}(\mathbf{x}) &= e_{ijk0}\exp(\gamma x_1) \\ h_{ij}(\mathbf{x}) &= h_{ij0}\exp(\gamma x_1), \end{aligned} \tag{46}$$

where c_{ijkl0}, e_{ijk0} and h_{ij0} correspond to the material parameters used in the previous examples. The influence of the material gradation on the stress intensity factor and electrical displacement intensity factor is analyzed. One can observe a strong influence of material gradation on the SIF in the conducting PE cracked specimen (Fig. 15).

For a gradation of mechanical material properties with x_1 coordinate and a uniform mass density, the wave propagation is growing with x_1. Therefore, the peak value of the SIF is reached in a shorter time instant in the functionally graded PE material (FGPM) than in a homogeneous one. The maximum value of the SIF is only slightly decreased for the FGPM cracked strip.

In the non-stationary case a pure mechanical load can induce a finite electric displacement intensity factor. The temporal variation of the EDIF in the cracked conducting PE strip is presented in Fig. 16. The character of the EDIF curve is similar to the SIF in FGPM specimen. The maximum value of the EDIF is larger for the FGPM than in the corresponding homogeneous material.

6. Conclusions

The MLPG method has been developed for general 2-D crack problems in functionally graded conducting piezoelectric solids. Both stationary and transient dynamic conditions are considered. Our numerical results for stationary conditions reveal that initial density of electrons (carriers of electric charge in *n*-type piezoelectric semiconductors) has only moderate influence on the crack displacement. However, the induced electric potential is strongly affected by the initial electron density. The largest value of the induced electric potential is achieved for a non-conducting piezoelectric material. For the cracked specimen under pure electric current load, the initial electron density also has a large influence on the crack displacement. A larger M_0 would induce a smaller crack displacement and density of electrons, but a larger electric potential.

Furthermore, the initial electron density has no influence on the stress intensity factor (SIF) for a crack under pure mechanical load. In non-stationary case, a pure mechanical load would also induce a finite EDIF. For non-conducting PE, the character of the EDIF curve is similar to the SIF. For the central crack specimen case, the value of the EDIF in the conducting material is reduced as compared to the non-conducting PE. However, for the edge crack specimen, the EDIF in the conducting PE is slightly larger. Generally, the EDIF in the cracked specimen is strongly dependent on both the boundary conditions and the specimen geometry. Furthermore, interaction of waves could enhance or reduce the EDIF in the conducting specimen, since electric fields are strongly dependent on the conductivity of PE. A quite simple conclusion can be made for cracked specimen under pure electric load: The SIF and EDIF are reduced in the conducting PE specimen case.

In the functionally graded PE material (FGPM), the peak value of the SIF is reached in a shorter time instant than in a homogeneous one. The maximum value of the SIF is only slightly reduced for the FGPM cracked strip. However, the maximum value of the EDIF is larger for the FGPM than in the corresponding homogeneous material.

Acknowledgments

The authors gratefully acknowledge the supports by the Slovak Science and Technology Assistance Agency registered under number APVV-0014-10 and the Slovak Grant Agency VEGA-2/0011/13.

References

Atluri, S.N., 1986. Energetic approaches and path-independent integrals in fracture mechanics, Chapter 5. In: Atluri, S.N. (Ed.), Computational Methods in the Mechanics of Fracture. North-Holland, Amsterdam, pp. 121–165.
Atluri, S.N., 2004. The Meshless Method, (MLPG) for Domain & BIE Discretizations. Tech Science Press, Forsyth.
Auld, B.A., 1973. Acoustic Fields and Waves in Solids. John Wiley and Sons, New York, pp. 357–382.
Bui, Q.T., Zhang, Ch., 2012. Extended finite element simulation of stationary dynamic cracks in piezoelectric solids under impact loading. Comput. Mater. Sci. 62, 243–257.
Busse, L.J., Miller, J.G., 1981. Response characteristics of a finite aperture, phase insensitive ultrasonic receiver based upon the acoustoelectric effect. J. Acoust. Soc. Am. 70, 1370–1376.
Davi, G., Milazzo, A., 2001. Multidomain boundary integral formulation for piezoelectric materials fracture mechanics. Int. J. Solids Struct. 38, 2557–2574.
Enderlein, M., Ricoeur, A., Kuna, M., 2005. Finite element techniques for dynamic crack analysis in piezoelectrics. Int. J. Fract. 134, 191–208.
Fleming, M., Chu, Y.A., Moran, B., Belytschko, T., 1997. Enriched element-free Galerkin methods for crack tip fields. Int. J. Numer. Methods Eng. 40, 1483–1504.
Garcia-Sanchez, F., Saez, A., Dominguez, J., 2005. Anisotropic and piezoelectric materials fracture analysis by BEM. Comput. Struct. 83, 804–820.
Garcia-Sanchez, F., Zhang, Ch., Sladek, J., Sladek, V., 2007. 2-D transient dynamic crack analysis in piezoelectric solids by BEM. Comput. Mater. Sci. 39, 179–186.
Govorukha, V., Kamlah, M., 2004. Asymptotic fields in the finite element analysis of electrically permeable interfacial cracks in piezoelectric bimaterials. Arch. Appl. Mech. 74, 92–101.
Gross, D., Rangelov, T., Dineva, P., 2005. 2D wave scattering by a crack in a piezoelectric plane using traction BIEM. SID: Struct. Integrity Durability 1, 35–47.
Gruebner, O., Kamlah, M., Munz, D., 2003. Finite element analysis of cracks in piezoelectric materials taking into account the permittivity of the crack medium. Eng. Fract. Mech. 70, 1399–1413.
Heyman, J.S., 1978. Phase insensitive acoustoelectric transducer. J. Acoust. Soc. Am. 64, 243–249.
Houbolt, J.C., 1950. A recurrence matrix solution for the dynamic response of elastic aircraft. J. Aeronaut. Sci. 17, 371–376.
Hu, Y., Zeng, Y., Yang, J., 2007. A mode III crack in a piezoelectric semiconductor of crystals with 6 mm symmetry. Int. J. Solids Struct. 44, 3928–3938.
Hutson, A.R., White, D.L., 1962. Elastic wave propagation in piezoelectric semiconductors. J. Appl. Phys. 33, 40–47.
Kuna, M., 2006. Finite element analyses of cracks in piezoelectric structures – a survey. Arch. Appl. Mech. 76, 725–745.
Lancaster, P., Salkauskas, K., 1981. Surfaces generated by moving least square methods. Math. Comput. 37, 141–158.
Lei, J., Wang, H., Zhang, Ch., Bui, Q.T., Garcia-Sanchez, F., 2014. Comparison of several BEM-based approaches in evaluating crack-tip field intensity factors in piezoelectric materials. Int. J. Fract. 189, 111–120.
Liu, P., Yu, T.T., Bui, Q.T., Zhang, Ch., Xu, Y.P., Lim, C.W., 2014. Transient thermal shock fracture analysis of functionally graded piezoelectric materials by the extended finite element method. Int. J. Solids Struct. 51, 2167–2182.
Liu, G.R., Dai, K.Y., Lim, K.M., Gu, Y.T., 2002. A point interpolation mesh free method for static and frequency analysis of two-dimensional piezoelectric structures. Comput. Mech. 29, 510–519.
Liu, P., Yu, T.T., Bui, Q.T., Zhang, Ch., 2013. Transient dynamic crack analysis in non-homogeneous functionally graded piezoelectric materials by the X-FEM. Comput. Mater. Sci. 69, 542–558.
Nayroles, B., Touzot, G., Villon, P., 1992. Generalizing the finite element method. Comput. Mech. 10, 307–318.
Ohs, R.R., Aluru, N.R., 2001. Meshless analysis of piezoelectric devices. Comput. Mech. 27, 23–36.
Pak, Y.E., 1990. Crack extension force in a piezoelectric material. ASME J. Appl. Mech. 57, 647–653.
Pak, Y.E., Herrmann, C.T., 1986. Conservation laws and the material momentum tensor for the elastic dielectric. Int. J. Eng. Sci. 24, 1365–1374.
Pan, E., 1999. A BEM analysis of fracture mechanics in 2D anisotropic piezoelectric solids. Eng. Anal. Boundary Elem. 23, 67–76.
Park, S.B., Sun, C.T., 1995. Effect of electric field on fracture of piezoelectric ceramics. Int. J. Fract. 70, 203–216.

Parton, V.Z., Kudryavtsev, B.A., 1988. Electromagnetoelasticity, Piezoelectrics and Electrically Conductive Solids. Gordon and Breach Science Publishers, New York.

Paulino, G.H., Jin, Z.H., Dodds, R.H., 2003. Failure of functionally graded materials. In: Karihaloo, B., Knauss, W.G. (Eds.), Comprehensive Structural Integrity, vol. 2. Elsevier Science, pp. 607–644.

Sheng, N., Sze, K.Y., 2006. Multi-region Trefftz boundary element method for fracture analysis in plane piezoelectricity. Comput. Mech. 37, 381–393.

Sladek, J., Sladek, V., Zhang, Ch., Solek, P., Pan, E., 2007. Evaluation of fracture parameters in continuously nonhomogeneous piezoelectric solids. Int. J. Fract. 145, 313–326.

Sladek, J., Sladek, V., Solek, P., Pan, E., 2008. Fracture analysis of cracks in magneto-electro-elastic solids by the MLPG. Comput. Mech. 42, 697–714.

Sladek, J., Sladek, V., Zhang, Ch., Wünsche, M., 2010. Crack analysis in piezoelectric solids with energetically consistent boundary conditions by the MLPG. CMES – Comput. Model. Eng. Sci. 68, 185–220.

Sladek, J., Sladek, V., Wünsche, M., Zhang, Ch., 2012. Analysis of an interface crack between two dissimilar piezoelectric solids. Eng. Fract. Mech. 89, 114–127.

Sladek, J., Stanak, P., Han, Z.D., Sladek, V., Atluri, S.N., 2013. Applications of the MLPG method in engineering & sciences: a review. CMES – Comput. Model. Eng. Sci. 92, 423–475.

Suresh, S., Mortensen, A., 1998. Fundamentals of functionally graded materials. Institute of Materials, London.

White, D.L., 1962. Amplification of ultrasonic waves in piezoelectric semiconductors. J. Appl. Phys. 33, 2547–2554.

Yang, J., 2005. An anti-plane crack in a piezoelectric semiconductor. Int. J. Fract. 136, L27–L32.

Yang, J.S., Zhou, H.G., 2005. Amplification of acoustic waves in piezoelectric semiconductor plates. Int. J. Solids Struct. 42, 3171–3183.

Zhu, T., Zhang, J.D., Atluri, S.N., 1998. A local boundary integral equation (LBIE) method in computational mechanics, and a meshless discretization approach. Comput. Mech. 21, 223–235.